Journal of Materials Chemistry B

Accepted Manuscript

ROYAL SOCIETY OF CHEMISTRY

www.rsc.org/materialsB

Journal of Materials Chemistry B RSCPublishing

ARTICLE

Two-photon Fluorescent *Bombyx Mori* Silk by Molecular Recognised Functionalization

Cite this: DOI: 10.1039/xoxxoooooox

Naibo Lin,[abc] Guoyang William Toh,[c] Yan Feng,[a] X.Y. Liu,*[abc] and Hongyao Xu*[a]

Received ooth January 2012,
Accepted ooth January 2012

DOI: 10.1039/xoxxoooooox

www.rsc.org/

Two-photon fluorescence (TPF) *Bombyx Mori* silk fibers were acquired for bioimaging by molecular recognised functionalization. In this context, 2,7-bis((E)-4-((E)-4-nitrostyryl)styryl)-9,9-dioctyl-9H-fluorene (**NF**) was adopted to functionalize silkworm silk fibers. **NF** exhibits a large two-photon absorption cross section, but has a low TPF quantum yield in the solid form due to the side-by-side (π-π) molecular stacking. In terms of the molecular recognition between the nitro groups of **NF** and the amide groups of silk fibroin, the silk fibers acquire the two-photon fluorescent emission with a significant enhancement for 350% in TPF quantum yield of **NF** molecules, compared with the solid state. In comparison, two molecules, 2,7-bis((*E*)-4-methylstyryl)-9,9-dioctyl-9*H*-fluorene (**MF1**), and 2,7-bis((*E*)-4-((*E*)-4-methylstyryl)styryl)-9,9-dioctyl-9*H*-fluorene (**MF2**), were selected for similar experiments. The later shows little effect due to the lack of molecular recognition. The TPF silk scaffolds were obtained, and the high quality imaging of **NF** in cell culture was finally achieved, which exerts extremely relevant implication in biomedical applications.

Introduction

Bioimaging becomes increasingly important in recent years.[1] In tissue engineering, the study of the structure, organization and evolvement of the scaffolds *in vivo* or *in vitro* is extremely crucial.[2] The conventional imaging techniques, such as scanning electron microscopy (SEM) and transmission electron microscopy (TEM), although of very high resolution (SEM < 1 nm, and TEM < 0.1 nm.), they can only be used for *ex-situ* observation.[3] However, these techniques are not capable of providing characterization and monitoring the growth of a tissue in real-time. These problems can be resolved to a certain extent by using *in-situ* observation techniques such as micro-CT and magnetic resonance imaging (MRI) techniques. However, both have their own disadvantages. The former one suffers from relatively low resolution (1-2 microns),[4] it requires a dense tissue sample for achieving a reasonably good contrast, and it can quite easily cause radiation damage in the sample.[5] On the other side, MRI uses non-ionizing radiation and is capable of imaging thin slices of tissue in any orientation at any depth. However, the application of this technique for high quality imaging is considerably limited by quite low resolution (~ 3 μm).[6] One-photon fluorescent microscopy is a possible technology available for single molecule analysis, apart from the issues of invasive excited UV light and the limited depth.[7] Recently, the use of two-photon fluorescence (TPF) microscope for biological imaging has received extensive interest because of several major advantages over current detection systems.[8] This exciting light of TPF microscope is located in the biologically transparent spectral range 800-1000 nm, and is therefore able to penetrate more deeply into biological tissues in non-invasive and real-time manner.[9] Meanwhile, the excitation probability is proportional to the square of the laser flux, with virtually no excitation outside the laser focal volume. This enables the precise spatial imaging for the microstructure of cell tissue. In this sense, this technology will fulfill the demands of high quality scaffold imaging.

To achieve the TPF high quality and omnidirectional imaging, the scaffolds need to be functionalized by TPF molecules. Meanwhile, the distributed TPF molecules have large two-photon absorption (TPA) cross section and high efficiency.[10] However, one should bear in mind that TPF quenching in scaffold caused by molecules aggregation may affect the feasibility of scaffold imaging. This is due to the known fact that most TPF molecules tend to aggregate via the π-π stacking, which usually results in a dramatic decrease of the TPF quantum yield.[11] To overcome above problem, various approaches have been developed to frustrate the fluorescence quenching. This includes designing a molecule with a distorted structure,[12] the attachment of steric hindrance groups,[13] and increasing the branches/dimensionality of the molecules.[14] Nevertheless, those methods still don't satisfy the high-level and special requirement in the TPF bioimaging applications.[15]

Bioscaffold is a kind of biocompatible and bioresorbable materials with 3D structure, which can provide space and nourishment for tissue regeneration.[16] The scaffold will degrade over time and promote the growth of new tissue. TPF microscopy would be one of the best choices for monitoring the evolution of bioscaffold in non-invasive, real time manner. Silk scaffolds have been attracting a great deal of interest in the biomedical fields,[17] notably in tissue engineering, due to their intrinsic functions, such as *in vitro* and *in vivo* biocompatibility,[18] robust mechanical properties,[19] and relatively slow proteolytic biodegradation.[20] Here, we take silk scaffold as an example to realize the analytic technique for TPF imaging of bioscaffold (Fig. 1a). The highlight of this paper is to achieve silk scaffold with high fluorescence efficiency by taking advantage of the molecular recognition of TPF and silk fibrin molecules. In this regard, the molecular recognition between silk fibroin molecules and TPF molecules between amide (NH) and nitro (NO_2) groups could decouple the π-π stacking TPF molecules, so that the annealed TPF would be "turned on".

Journal of Materials Chemistry B RSCPublishing

ARTICLE

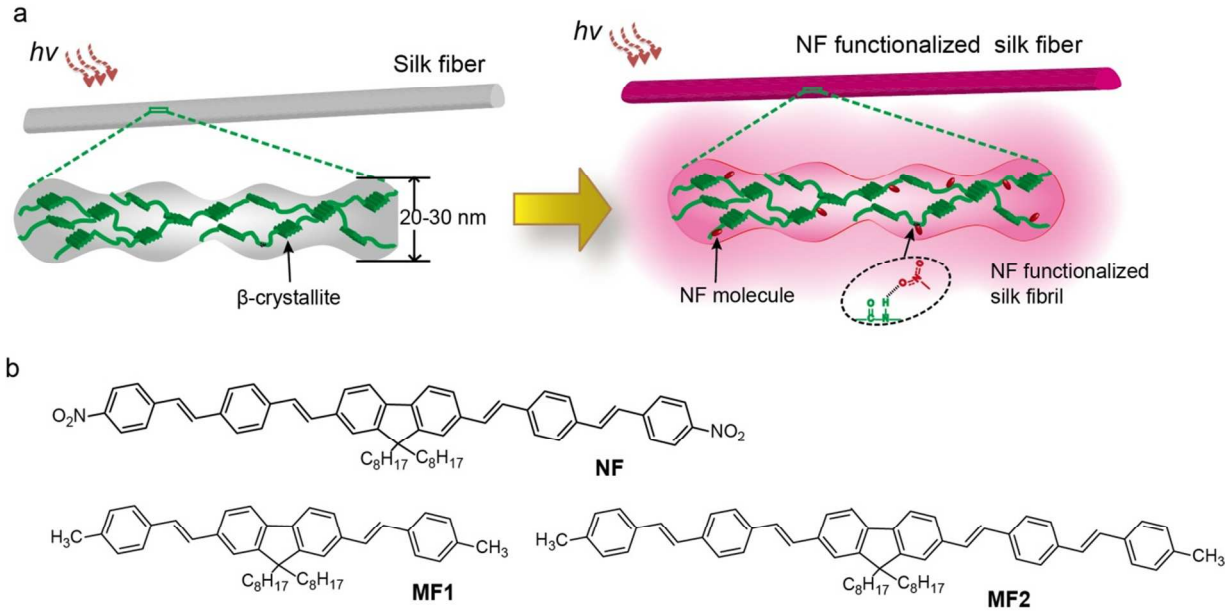

Fig. 1 a) Proposed model for the silk fibril decoupling effect by the molecular recognition of 2,7-bis((*E*)-4-((*E*)-4-nitrostyryl)styryl)-9,9-dioctyl-9*H*-fluorene (**NF**) molecules. Two-photon fluorophores **NF** were decoupled by their specific binding with the amide groups in the silk fibroin molecules by means of hydrogen bonds. b) Molecular structures of **NF**, **MF1**, and **MF2**.

Results and discussion

Synthesis and characteristics of two-photon molecules

The TPA cross section of the organic stainers in scaffolds is one of the critical factors for TPF imaging, which can be increased by lengthening the π-conjugation, and improving the symmetry and donor-acceptor intensity of the organic molecule.[21] Fluorene has a large electron delocalization conjugated plane with two benzene rings, fused by a five-member ring with several active positions. To obtain large TPA cross-section, the π-conjugation on the fluorene core can be elongated by vinylbenzene at two para positions 2 and 7 to form the larger symmetrical structures. Furthermore, two terminals of fluorene derivatives can be connected with special functional groups to explore the effect for enhancing the TPA cross section and TPF quantum yield. In addition, fluorene is a conventional staining agent with low toxicity for living cell.[22] Taking this into account, we synthesized three fluorene compounds containing different substitutional groups, namely, 2,7-bis((*E*)-4-((*E*)-4-nitrostyryl)styryl)-9,9-dioctyl-9*H*-fluorene (**NF**) 2,7-bis((*E*)-4-methylstyryl)-9,9-dioctyl-9*H*-fluorene (**MF1**), and 2,7-bis((*E*)-4-((*E*)-4-methylstyryl)styryl)-9,9-dioctyl-9*H*-fluorene (**MF2**) (Fig. 1b).

The UV-Vis absorption spectra of **NF**, **MF1**, and **MF2** molecules in THF (tetrahydrofuran) are given in Fig. 2. The absorption maximum of **MF1** is located at 374 nm. The absorption spectrum of **MF2** has the maxima at 406 nm. Comparing the absorption peaks of **MF1** and **MF2**, 32 nm red shift was found, indicating that the latter has a longer conjugation length than the former one. The absorption maximum of **NF** is red-shifted compared to that of **MF2**, which is due to the electron withdrawing ability and better electron delocalization of the terminal nitro group in **NF**.

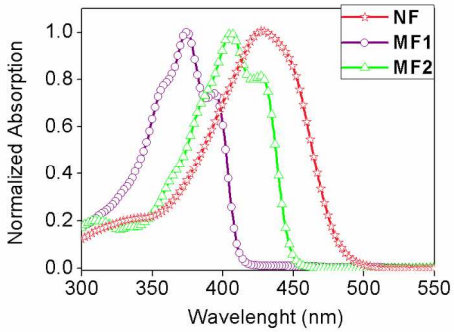

Fig. 2 UV-Vis absorption spectra of **NF**, **MF1**, and **MF2** in THF at concentration 1.0×10^{-6} M. The spectra are normalized at their peak wavelengths.

Z-scans measurements were carried out to evaluate the TPA processes and properties of all compounds using ultrafast 450 fs laser pulses at 1-kHz repetition rate. To prevent the deviation of the measured TPA cross-section values from the intrinsic TPA process caused by the potential accumulative thermal scattering effects and exited-states absorption, a relatively low intensity range was employed to detect the samples at concentration of 1.0×10^{-4} M.

From Fig. S1, it can be found that the measured TPA cross-section values of **NF**, obtained from the best fits between the TPA theory and Z-scan data, remain nearly constant in a straight line across the irradiance range from 58.5 to 116.9 GW·cm^{-2} within the experimental errors, confirming the independence of the laser intensity. This indicates the observed nonlinear absorption is induced from a pure TPA process. Other nonlinear mechanisms such as thermally induced scattering and excited-state absorption, in particular singlet excited-state absorption, are negligible in our experiments. Other molecules exhibit similar behavior. It can be seen that the TPA cross-section of 1886 GM for **NF** is considerably higher than 905 GM for **MF2**, greater than **MF1** (σ = 506 GM). All of them are higher than the conventional TPA dye, rhodamine 6G, which is about 100 GM.[23] Large TPA cross-section of **NF** molecules in THF can be attributed to the significant role of the strong polarization effect between electron accepted group NO_2 and π-conjugation moieties in their molecular structure.[24]

Preparation of two-photon silk fibers/scaffolds and the mechanical properties

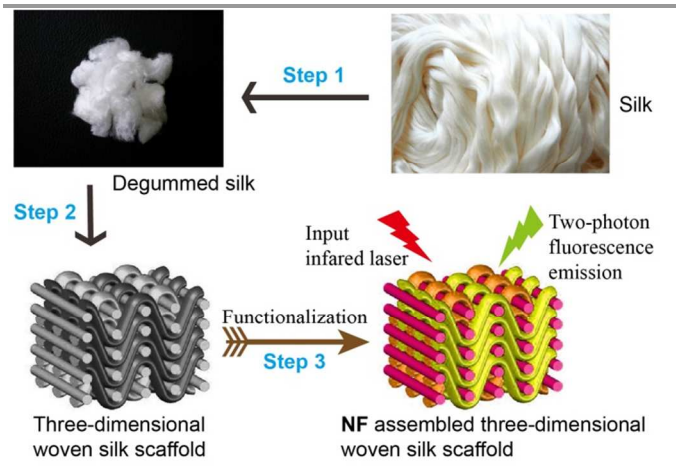

Fig. 3 Preparation process of two-photon silk scaffolds.

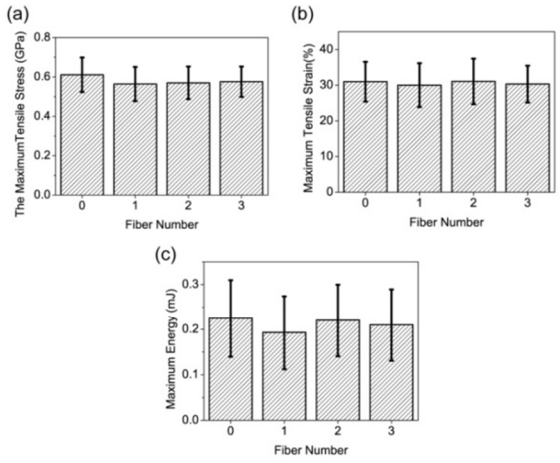

Fig. 4 Mechanical properties of *Bombyx mori* silk (Fiber Number 0), **NF**, **MF1**, and **MF2** modified silk fibers (Fiber Number 1-3). a) Relationship between maximum the breaking stress and fiber number, b) Relationship between maximum tensile strain and fiber number, c) Relationship between maximum energy and fiber number

The TPF silk fibers were achieved via assembling **NF**, **MF1**, and **MF2** into silk fibers. The *Bombyx mori* silk fibers were from No. 2 Liang Guang. In our method, a proper amount of the fluorene compound was added into in dimethylsulfoxide (DMSO), and sonicated to make the solution homogenous. The *Bombyx mori* silk fibers/scaffolds were immersed into the solution and kept in it for about 40 minutes at 80 ^{o}C. This procedure resulted in the swollen sample, which was then taken out of the solution and allowed DMSO to evaporate at room temperature. This treatment leads to the absorption of TPF molecules into the silk fibrils and at the same time gives rise to the cooperative assembly between TPF molecules and the silk fibroin (Fig. 3).

To check whether the assembly process may exert any impact on the mechanical property of the silk fibers, the mechanical properties of the modified silk were compared to the unmodified one. The results of the comparison between the two are shown in Fig. 4. It is quite obvious that the properties such as the breaking stress, the breaking strain, and the breaking energy of the functionalized silk fibers exhibit no much difference from the comparative *Bombyx mori* silk fibers. In other words, the treatment does not deteriorate the mechanical properties of the original Bombyx mori silk fibers. From the SEM images of the functionalized silk fibers (Fig. 5), it can be seen that diameters and surface morphologies of comparative degummed silks and functionalized silk fibers exhibit no difference. This is additional evidence that the functionalization process did not jeopardize the basic properties of the silk fibers.

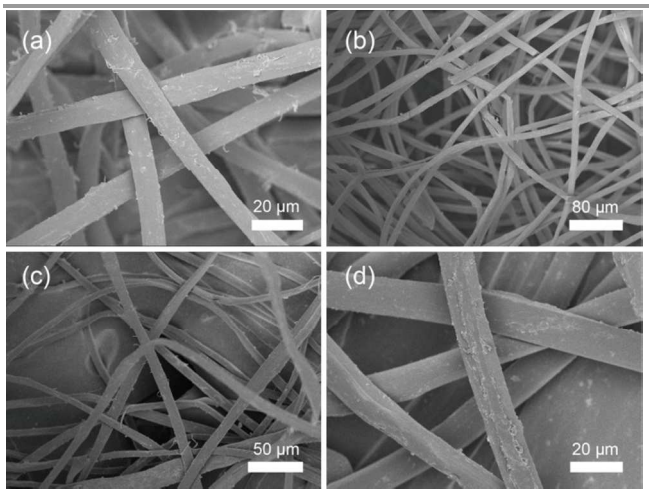

Fig. 5 Scanning electron microscope of silk fibers modified with a) **NF** silk fiber, b) **MF1** silk fiber, c) **MF2** silk fiber, and d) control silk fibers.

Mechanism of fluorescence enhancement

When a solid state sample was illuminated with a UV lamp, **NF** emitted very week light, but on the other side the emitted light from the **NF** fibers was very strong, which indicates that the dissociation formation in the latter one enhanced the light emission considerably. To verify these observations, one-photon fluorescence properties of **NF**, **MF1**, and **MF2** in solid state (powder) and in the respective liquid states (each dissolved in THF), as well as in silk fibers were characterized. The quantum yield values of the solid were determined using an integrating sphere (ISF-513). It's found that in solid state the process of π-π stacking usually leads to the decrease of the fluorescence quantum yield and the red-shift of the fluorescence spectrum.[13a, 25] Comparison of the quantum yield of **NF** in solid states and in the silk fibers, it can be found that while the

quantum yield of **NF** in the solid states is as low as 8%, the **NF** is boosted to 28% by assembling to silk fiber. It becomes clear that the assembling of **NF** to the silk fibroin enhanced the **NF** fluorescence emission. The structure of **MF2** is identical to **NF** except the fact that the terminal group $-NO_2$ in **NF** is replaced by $-CH_3$ in **MF2**. After incorporating into silk fibers, the quantum yield of **MF2** in silk fibers (14%) remains, almost no change compared with those in the solid form (10%). Quantum yield change of **MF2** from in powder state to in silk fibers is obviously different from that of **NF**, which confirms that the fluorescence emission enhancement is caused by the nitro ($-NO_2$) terminal groups of **NF** molecules. Nitro groups have strong polar bonds, which can interact effectively with the amide groups of silk fibroins by hydrogen bonds. Hence, we can predict that the nitro groups act as anchors, which can prevent the π-π stacking of conjugated bridge. To further verify the interaction which makes the quantum yield jump up, the quantum yields of **MF1** in solid form and in silk fiber were characterized, the results (12% in solid form, 15% in silk fiber) show the similar behaviour to **MF2**.

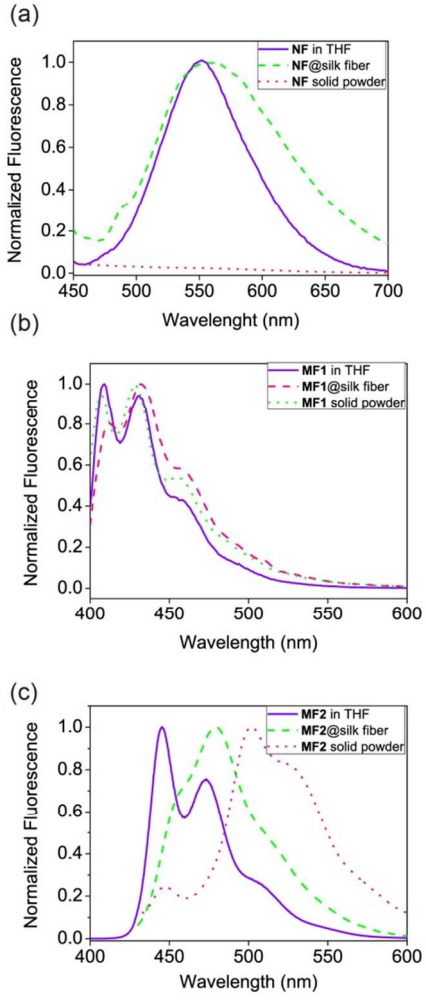

Fig. 6 One-photon fluorescence spectra of **NF**, **MF1**, and **MF2** in THF solution, assembled in silk fibers and in solid powder form.

As shown in Fig. 6a, it is surprisingly to see that **NF** fabrics reveal intense fluorescence, while the emission from **NF** powders is very weak and hardly detectable (the maximum fluorescence spectra of the **NF** powder cannot be identified). This reflects the molecular aggregation difference at different states. **NF** molecules in the powder form exhibit a stronger dipole-dipole and π-π interaction. The interactions lead to the aggregation between **NF** molecules, which anneal the fluorescence emission. In the **NF** functionalized fibers, the binding of **NF** molecules to silk fibrils dissociates the π-π stacking **NF** molecules, which eliminates the fluorescence annealing in the dry powder state, therefore, enhances the fluorescence emission by functionalized silk fibroin fibers. The maxima of the **NF** powder in silk fiber is almost the same as that of **NF** powder in THF solution. As we known, π-π stacking of fluorescence molecules in good solvent can be eliminated. It can be inferred that π-π stacking of **NF** is dissociated well by the protein of silk fiber. **MF1** has small conjugated bridge and relative long alkyl chain on the position 9 of fluorine, π-π stacking of **MF1** would not be as strong as **NF**. The fact is that **MF1** is not a good candidate to be used. Indeed, a close inspection of Fig. 6b, shows that there are no obvious shifts of the fluorescence peaks of **MF1** fibers compared with those in solution and in solid powder form, suggesting that this material is not a good candidate to be used as TPF agent. On the other side, the fluorescent curves of the **MF2** solution, **MF2** fibers, and the powders exhibit a monotonous bathochromic shift in the following order; **MF2** solution < **MF2** fibers < **MF2** powder (Fig. 6c). Compared with **MF1**, **MF2** has longer conjugated bridge and lower quantum yield, which implies that the intermolecular interactions between silk fibroins and **MF2** create better de-aggregation effect than **MF1**. However, both of the intermolecular interactions are weaker than in **NF**.

Two-photon action cross section was characterized by $\sigma\eta$, where σ is the TPA cross section and η is the fluorescence quantum yield. These parameters were used to evaluate the overall TPF performance. Using the previously determined values for σ and η, the product of the two was determined for **NF** in the solid form and **NF** silk fibers. The $\sigma\eta$ values for the former one was relatively low, $\sigma\eta_{solid}$ = 1886 × 0.08 = 150 GM, while for the latter one was strikingly bigger, $\sigma\eta_{fiber}$ = 1886 × 0.28 = 528 GM. A comparison between the corresponding $\sigma\eta$ values indicates clearly that enhancement of TPF for **NF** silk fibers is more than 3.52 times bigger than that for **NF** in the solid form. On the other side, the $\sigma\eta$ values for **MF1** and **MF2** silk fibers are 76 GM and 126 GM, respectively. Therefore, the **NF** silk fibers exhibit much higher TPF property, even though the quantum yield is very low in solid form. Hence, the **NF** silk scaffolds are most promising candidate for TPF imaging.

Two-photon fluorescence silk scaffolds for bioimaging

Since the uniformity of the fluorescence emission of silk scaffolds is one of the key features for TPF bioimaging, a TPF confocal microscopy was employed to study the functionalized silk fibers (at the wavelength of exciting light λ = 800 nm). For this purpose, precise images of optical slices of the **NF** functionalized silk fibers are given in Fig. S2. These images show that the TPF emission from both the surface and the centers of the silk fibers were observed. This indicates that **NF** molecules were distributed evenly into the bulk of silk fibers and interact strongly with the alkyl chains in the silk fibrous proteins chains in terms of the nitro group in **NF**. However, the TPF of **MF1**, and **MF2** fibers mainly occurs near the surface of the silks, which reveals their week absorbability and dispersibility in the silk fibers (c.f. Fig. S3). This suggests that **NF** is likely to be the most attractive TPF molecule for functionalization.

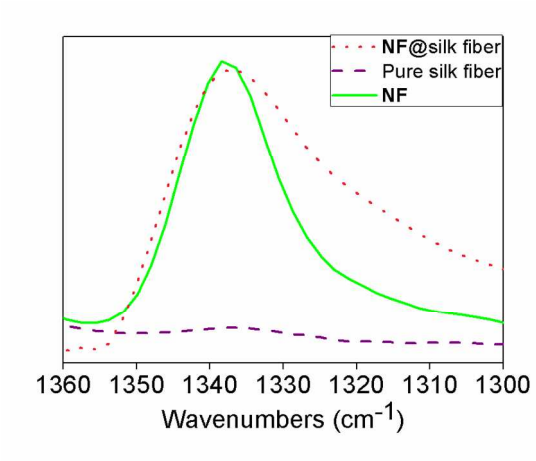

Fig. 7 FTIR spectra of control silk fiber, **NF** and the mixture of **NF** and silk fibroin fiber (mass ratio: 1:1)

As an additional support that **NF** molecules can be distributed evenly into the silk, we take FTIR spectra of the **NF** silk fiber in the same wavelength region (1360 - 1300 cm^{-1}) as that used to examine pure silk fibers, **NF** powder and the mixture of **NF** and silk fibroin fiber (mass ratio: 1:1). It was confirmed in literature that adulterant manifests a good dispersion in polymer matrix if a relatively strong attractive interaction between polymer and adulterant is introduced.[26]

Silk fiber is an amphiphilic block co-polymer with the molecular mass of the dominant high molecular weight protein of ~390 KDa[27]. The dominating hydrophobic peptide repeats self-organization into the β-sheet structures, which were connected by hydrophilic noncrystal regions[28]. After the assembly treatment, β-sheet structures remained while the hydrophilic block of the silk fibroin may make it a potential dispersing agent for two-photon molecules. It is known that the hydrophilic chains in the non-crystal region are rich in amide groups, which can provide NH. Therefore, the two-photon molecules should have polar group to interact with silk fibroin to fulfill the demands for the strong attractive interaction. As shown in Fig. 7, **NF** shows a characteristic nitro vibration band centered at 1340 cm^{-1}. After **NF** is incorporated into the silk fibers, this maximum absorption shifts slightly toward a lower frequency (a lower wavenumber). As the frequency shift of FTIR is much related to the interaction between the functional molecules, the increase of absorbance frequency is due to the hydrogen bond interaction.[29] Evidently, silk fibroin provides some NH groups to interact with the nitro group of **NF** by hydrogen bonds. So the nitro group of **NF** is crucial to control the distribution of **NF** in silk fibers. However, no obvious active groups were found for **MF1**, and **MF2** after they doped into silk, which accounts for their week intermolecular interaction with the silk fibers. As mentioned earlier, development of silk scaffolds with TPF properties is valuable for *in vitro* and *in vivo* imaging applications. According to the TPF quantum yield and uniformity, **NF** silk scaffolds seem to fulfill above biological imaging criteria.

To assess TPF bioimaging application for **NF** silk scaffolds, the cell culture experiments were applied. Three-dimensional TPF images of **NF** silk scaffolds were obtained by a laser scanning confocal microscope at the exciting wavelength of 800 nm. After sterilizing, 3T3 fibroblast cells were seeded and grown on the silk fibroin scaffolds for ten days. TPF images were taken after the cells were stained with Alexa Fluor® 488 phalloidin and 4',6-diamidino-2-phenylindole (DAPI) to show normal growth of the cells on the fibroin scaffold. The results are shown in Fig 8. The key features of them are: the **NF** scaffolds appear pink while the actin appears green, and nucleolus blue. The results show that the cells can grow well on **NF** silk scaffold, which infer that the modified silk scaffold is biocompatible. The clear interface between scaffold and cells allows convenient monitoring of scaffold. The results show that the silk scaffolds keep TPF emission well, which provide the possibility for the scaffolds imaging by advanced TPF technologies. TPF spectrum of the silk fabric scaffold shows maxima at around 573 nm (c.f. Fig. 8c). It is well known that the transition probability for TPF depends on the square of the incident light intensity[30]. TPF spectroscopy of the **NF** silk scaffold was obtained at different excitation intensities. Inset of Fig. 8c displays the log-log plots of the detected TPF intensity versus the excitation intensity. The emission signal of the **NF** silk scaffold is proportional to excitation intensity, and the slope is about 2, confirming the presence of the TPA process. The use of the TPF silk as a scaffold not only takes the advantage of TPF technologies, but also allows an improved visualization of cells.

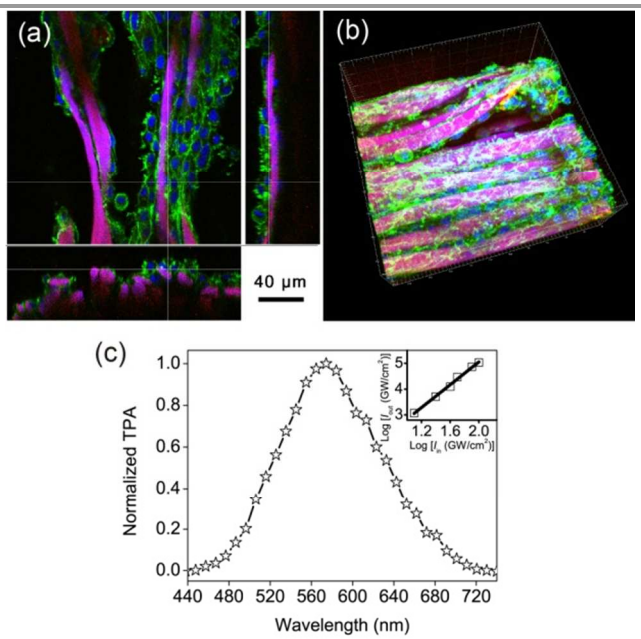

Fig. 8 a) TPF microscope image showing cross-sectional view of **NF** fabric scaffold and 3T3 fibroblast cells stained with Alexa Fluor® 488 phalloidin and 4',6-diamidino-2-phenylindole (DAPI) after culturing for ten days in culture medium. Excitation laser wavelength = 800 nm. b) Three-dimensional TPF images of **NF** silk scaffold and 3T3 fibroblast cells. c) Normalized TPF spectra of NF silk, Inset: Input-intensity-dependent TPF of **NF** silk fiber.

Conclusions

TPF compounds with large TPA cross-section were designed and synthesized to functionalize *Bombyx mori* silk fibers for TPF imaging. **NF** molecules in silk fibers exhibited a large TPA cross-section (1886 GM) and stable TPF evenly emitted from both the surface and the centers of the silk fibers, while good mechanical properties of pure silk fibers were maintained. The mechanism of fluorescence enhancement and monodispersion of **NF** in silk fibers is due to the molecular recognition between the nitro groups and silk fibroin. On the contrary, **MF1** and **MF2** cannot effectively overcome the aggregation effect due to the lack of molecular recognition between amide groups and CH_3 groups. This work provides a promising solution for the scaffolds imaging in a non-invasive, 3D and real time manner. The strategy of molecular recognition is not only limited between the **NF** molecules and silk protein, but can be

applied to the interaction of other materials, such as between functional molecules/quantum dots and other scaffolds. We can foresee a great demand to produce functional materials using molecular recognition that can be applied for tissue engineering scaffolds with biological electrical, optical and magnetic features.

Experimental Section

Preparation of two-photon fluorescence silk scaffolds

Silk scaffolds were waved from silk fibers, which were obtained from NO. 2 Liangguang *Bombxy mori* silkworm silk. Raw silk fibers were degummed in an aqueous solution containing 5g·L^{-1} sodium carbonate, 10 g·L^{-1} soap at 85^{o}C for 45 min, then rinsed throughout using DI water. The fibers were dried at room temperature for two days. In a typical process, silk fibers/scaffolds were immersed in a reaction bath with a dimethylsulfoxide (DMSO) solution (0.15 ml) consisting of 4% **NF** (on the weight of fibers [o.w.f.]). Then, the silk fibers/scaffolds were fished out and dry at room temperature. The functionalized silk fibers were rinsed with distilled water, and sonicated for 5 minutes. The same rinsing procedure was repeated for five times.

Cell culture and seeding.

Silk scaffolds were cut into cuboids (5 mm × 5 mm × 2 mm), sterilized using UV radiation, under laminar airflow chamber. These sterilized silk scaffolds were then transferred to a 24-well culture plates individually. 3T3 fibroblast cells were seeded onto the scaffolds at a density of 4 × 10^{5} cells per scaffold, and then cultured in Dulbecco's modified Eagle's medium (DMEM) supplemented with 10% fetal bovine serum (FBS), 3% D-(+)-Glucose, 1.5% sodium bicarbonate and 1% penicillin streptomycin solution (10.000 mg/ml) at 37^{o}C at 95% humidity and 5% CO_2. Cells were observed daily by microscopy and the cell culture medium was changed on a daily basis.

Two-photon fluorescence imaging.

Incubation of the cells was stopped after ten days, cell growth was examined with light microscopy and cells were fixed with 3.8% paraformaldehyde (PFA) for 15 minutes at room temperature. The cell membrane was permeabilized with 0.1% Triton X-100 in PBS for 5 minutes at room temperature. The samples were imaged by TPF microscope after incubating the samples in 0.4 mL PBS containing 10 µl Phalloidin-Alexa 488 and 4 µl 4',6'-di-amidino-2-phenyl-indol (DAPI) for 30 min, followed by extensive washing at 200 rpm for 45 mins.

Physical characterization.

The FTIR spectra were recorded on a Thermo Nicolet 5700 spectrometer. The ^{1}HNMR spectra were recorded on a Bruker AVANCE/DMX 400-MHz Bruker NMR spectrometer using chloroform-*d* ($CDCl_3$). Tetramethylsilane was used as the internal reference for the NMR analyses. UV-vis spectra were recorded on a Varian cary 50 spectrometer with a 1-cm^{2} quartz cell. Fluorescence spectra were recorded on a JASCO FP-6600 spectrophotometer using a quartz cell with an optical path length of 1 mm. The quantum yield of the solid films were determined using an integrating sphere. Scanning electron microscopy images were recorded on a JEOL JSM-6700F field electron microscope operating at 5 kV. An Instron MicroTester was used to measure the force-extension characteristics of the silk. A thread was fixed between two hooks of the instrument, which had a gauge length of 20 mm with a measured error of 0.1 mm. The thread was stretched until it broke and the stain rate was 50% per minute. The experiments were operated at 22^{o}C and humidity was kept at 65%.

TPF measurement of organic compounds was carried out using the same laser system described above operating at 780 nm. The details of the two-photon technique experimental setup are described elsewhere. TPF imaging and spectrum of fibers were performed using Leica TCS SP2 laser scanning confocal microscope with a Ti:Sapphire laser (Mira Optima 900F, Coherent) as the excitation source. For all experiments, the laser is tuned at 800 nm with 0.5 mW power after the objective and provides ~100 fs pulses at a repetition rate of 76 MHz.

TPA cross-section values for all dyes were determined by open-aperture Z-scan measurements at 780 nm with 450-fs laser pulses at 1-kHz repetition rate. The laser beam was generated by a mode-locked Ti: Sapphire laser, which was seeded a Ti: Sapphire regenerative amplifier. The laser pulses with near-Gaussian spatial and temporal profiles were focused onto 1-mm-thick quartz cuvette using a lens of focal length of 15 cm. Moreover, the Z-scan experimental system was calibrated using a piece of cadmium sulfide bulk crystal because this sample possesses large TPA at the wavelength of 780 nm and was well-investigated in our laboratory. In theory, the normalized transmittance for the open aperture can be written as

$$T(z, s = 1) = \sum_{m=0}^{\infty} \frac{[-q_0(z)]^m}{(m+1)^{3/2}}, \text{for } |q_0| < 1 \qquad (1)$$

where $q_0(z) = \beta I_0 L_{eff}/(1+z^2/z2\ 0)$ with β is the TPA coefficient, I_0 is the intensity of laser beam at focus ($z = 0$), $L_{eff} = [1-\exp(-\alpha L)]/\alpha$ is the effective thickness (α is the linear absorption coefficient, L is the sample thickness, z_0 is the diffraction length of the laser beam, and z is the sample position).[31] The TPA cross-section σ is calculated by

$$\sigma = h\nu\beta/N \qquad (2)$$

where N is the number of molecules per cm^{3} and $h\nu$ is the excitation photon energy. The TPA cross-section σ is expressed in Göppert Mayer (GM) units, in which 1 GM = 1×10^{-50} cm^{4} s photon^{-1}.

TPF imaging and spectrum of fibers were performed using Leica TCS SP2 laser scanning confocal microscope with a Ti:Sapphire laser (Mira Optima 900F, Coherent) as the excitation source. For all experiments, the laser is tuned at 800 nm with 0.5 mW power after the objective and provides ~100 fs pulses at a repetition rate of 76 MHz. The silk sample sealed in test tubes were carried out at 80 ^{o}C for about 40 mins. Then, the silk fibers/scaffolds were fished out and rinsed with distilled water, and sonicated for 5 mins. The same rinsing procedure was repeated for five times. The obtained fibers/scaffolds were dried later at room temperature.

Acknowledgements

This work is financially supported by AcRF Tier 1(R-143-000-497-112), National Nature Science Foundation (Nos. 21271040, 51073031), the Excellent Young Teachers Training Program of Shanghai (ZZyyy12001), Shanghai Institute of Technology Scientific Research Foundation for Introduced Talent (YJ2012-25)and Fundamental Research Funds for the Central Universities (ZK1018).
We appreciate Prof. R.I. Ristic from the University of Sheffield for the discussion and polishing of this paper.

Notes and references

[a] College of Material Science and Engineering & State Key Laboratory for Modification of Chemical Fibers and Polymer Materials, Donghua University, Shanghai, 201620, China.
[b] Research Institute for Biomimetics and Soft Matter & College of Materials, Xiamen University, Xiamen, 361005, China.

[c] MIT-Singapore Alliance, Department of Physics, National University of Singapore, 2 Science Drive 3, Singapore, 117542, Singapore.
* Corresponding author: Tel.: +65-6516 2812; Fax: +86-29-88322585
E-mail address: phyliuxy@nus.edu.sg (X. Y. Liu); hongyaoxu@dhu.edu.cn (H. Y. Xu)
Electronic Supplementary Information (ESI) available: Synthesis and characterization data of organic molecules. Two-photon fluorescence (TPF) image of **NF** scaffold and the images of **MF1** fiber. See DOI: 10.1039/b000000x/

1 (a) S. Berning, K. I. Willig, H. Steffens, P. Dibaj and S. W. Hell, *Science*, 2012, **335**, 551; (b) E. Betzig, G. H. Patterson, R. Sougrat, O. W. Lindwasser, S. Olenych, J. S. Bonifacino, M. W. Davidson, J. Lippincott-Schwartz and H. F. Hess, *Science*, 2006, **313**, 1642-1645; (c) S. T. Hess, T. P. K. Girirajan and M. D. Mason, *Biophys. J.*, 2006, **91**, 4258-4272; (d) M. J. Rust, M. Bates and X. Zhuang, *Nat. Methods*, 2006, **3**, 793-796.
2 Y. Y. Yang, S. M. Dorsey, M. L. Becker, S. Lin-Gibson, G. E. Schumacher, G. A. Flaim, J. C. Kohn and C. G. Simon, *Biomaterials*, 2008, **29**, 1901-1911.
3 W. L. Rice, S. Firdous, S. Gupta, M. Hunter, C. W. P. Foo, Y. Wang, H. J. Kim, D. L. Kaplan and I. Georgakoudi, *Biomaterials*, 2008, **29**, 2015-2024.
4 S. J. Schambach, S. Bag, L. Schilling, C. Groden and M. A. Brockmann, *Methods*, 2010, **50**, 2-13.
5 J. Giles, *Nature*, 2004, **431**, 391-391.
6 (a) H. Mamin, M. Poggio, C. Degen and D. Rugar, *Nature Nanotechnology*, 2007, **2**, 301-306; (b) H. H. Xu, S. F. Othman and R. L. Magin, *J. Biosci. Bioeng.*, 2008, **106**, 515-527; (c) J. V. Terrovitis, J. W. M. Bulte, S. Sarvananthan, L. A. Crowe, P. Sarathchandra, P. Batten, E. Sachlos, A. H. Chester, J. T. Czernuszka, D. N. Firmin, P. M. Taylor and M. H. Yacoub, *Tissue Eng.*, 2006, **12**, 2765-2775.
7 S. Weiss, *Science*, 1999, **283**, 1676-1683.
8 (a) W. Denk, J. Strickler and W. Webb, *Science*, 1990, **248**, 73-76; (b) M. Pawlicki, H. A. Collins, R. G. Denning and H. L. Anderson, *Angew. Chem. Int. Edit.*, 2009, **48**, 3244-3266; (c) G. S. He, L. S. Tan, Q. Zheng and P. N. Prasad, *Chem. Rev.*, 2008, **108**, 1245-1330; (d) F. Helmchen and W. Denk, *Nat. Methods*, 2005, **2**, 932-940; (e) N. B. Lin, Y. Feng, S. Y. Guang and H. Y. Xu, *Chin. Chem. Lett.*, 2011, **22**, 1257-1260.
9 (a) N. A. A. Rahim, W. McDaniel, K. Bardon, S. Srinivasan, V. Vickerman, P. T. C. So and J. H. Moon, *Adv. Mater.*, 2009, **21**, 3492-3496; (b) T. R. Krishna, M. Parent, M. H. V. Werts, L. Moreaux, S. Gmouh, S. Charpak, A. M. Caminade, J. P. Majoral and M. Blanchard Desce, *Angew. Chem. Int. Edit.*, 2006, **45**, 4645-4648; (c) H. M. Kim, M. J. An, J. H. Hong, B. H. Jeong, O. Kwon, J. Y. Hyon, S. C. Hong, K. J. Lee and B. R. Cho, *Angew. Chem. Int. Edit.*, 2008, **47**, 2231-2234; (d) J. Babin, M. Pelletier, M. Lepage, J. F. Allard, D. Morris and Y. Zhao, *Angew. Chem. Int. Edit.*, 2009, **48**, 3329-3332.
10 (a) J. Mertz, *Curr. Opin. Neurobiol.*, 2004, **14**, 610-616; (b) N. B. Lin, X. Y. Liu, Y. Y. Diao, H. Y. Xu, C. Y. Chen, X. H. Ouyang, H. Z. Yang and W. Ji, *Adv. Funct. Mater.*, 2012, **22**, 361-368.
11 (a) H. B. Fu, D. B. Xiao, J. N. Yao and G. Q. Yang, *Angew. Chem. Int. Edit.*, 2003, **42**, 2883-2886; (b) S. Sreejith, K. P. Divya and A. Ajayaghosh, *Chem. Commun.*, 2008, 2903-2905; (c) Z. Q. Xie, B. Yang, G. Cheng, L. L. Liu, F. He, F. Z. Shen, Y. G. Ma and S. Y. Liu, *Chem. Mater.*, 2005, **17**, 1287-1289; (d) S. Ozcelik and D. L. Akins, *J. Phys. Chem. B*, 1999, **103**, 8926-8929; (e) R. Deans, J. Kim, M. R. Machacek and T. M. Swager, *J. Am. Chem. Soc.*, 2000, **122**, 8565-8566; (f) M. Levitus, K. Schmieder, H. Ricks, K. D. Shimizu, U. H. F. Bunz and M. A. Garcia-Garibay, *J. Am. Chem. Soc.*, 2001, **123**, 4259-4265.
12 S. W. Thomas, G. D. Joly and T. M. Swager, *Chem. Rev.*, 2007, **107**, 1339-1386.
13 (a) H. Y. Woo, B. Liu, B. Kohler, D. Korystov, A. Mikhailovsky and G. C. Bazan, *J. Am. Chem. Soc.*, 2005, **127**, 14721-14729; (b) W. Z. Yuan, P. Lu, S. M. Chen, J. W. Y. Lam, Z. M. Wang, Y. Liu, H. S. Kwok, Y. G. Ma and B. Z. Tang, *Adv. Mater.*, 2010, **22**, 2159-2163.
14 (a) H. Y. Woo, D. Korystov, A. Mikhailovsky, T. Q. Nguyen and G. C. Bazan, *J. Am. Chem. Soc.*, 2005, **127**, 13794-13795; (b) J. S. Yang and J. L. Yan, *Chem. Commun.*, 2008, 1501-1512; (c) H. Zhang, Z. C. Cui, Y. Wang, K. Zhang, X. L. Ji, C. L. Lu, B. Yang and M. Y. Gao, *Adv. Mater.*, 2003, **15**, 777-780; (d) J. N. Moorthy, P. Natarajan, P. Venkatakrishnan, D. F. Huang and T. J. Chow, *Org. Lett.*, 2007, **9**, 5215-5218.
15 (a) T. Y. Yu, C. K. Ober, S. M. Kuebler, W. H. Zhou, S. R. Marder and J. W. Perry, *Adv. Mater.*, 2003, **15**, 517-521; (b) S. Putthanarat, R. K. Eby, R. R. Naik, S. B. Juhl, M. A. Walker, E. Peterman, S. Ristich, J. Magoshi, T. Tanaka, M. O. Stone, B. L. Farmer, C. Brewer and D. Ott, *Polymer*, 2004, **45**, 8451-8457; (c) C. C. Corredor, Z. L. Huang and K. D. Belfield, *Adv. Mater.*, 2006, **18**, 2910-2914.
16 (a) R. F. Service, *Science*, 2008, **322**, 1460-1461; (b) F. T. Moutos, L. E. Freed and F. Guilak, *Nat. Mater.*, 2007, **6**, 162-167.
17 (a) A. M. Collins, N. J. V. Skaer, T. Cheysens, D. Knight, C. Bertram, H. I. Roach, R. O. C. Oreffo, S. Von-Aulock, T. Baris, J. Skinner and S. Mann, *Adv. Mater.*, 2009, **21**, 75-78; (b) B. D. Lawrence, M. Cronin-Golomb, I. Georgakoudi, D. L. Kaplan and F. G. Omenetto, *Biomacromolecules*, 2008, **9**, 1214-1220.
18 C. Vepari and D. L. Kaplan, *Prog. Polym. Sci.*, 2007, **32**, 991-1007.
19 C. Y. Jiang, X. Y. Wang, R. Gunawidjaja, Y. H. Lin, M. K. Gupta, D. L. Kaplan, R. R. Naik and V. V. Tsukruk, *Adv. Funct. Mater.*, 2007, **17**, 2229-2237.
20 (a) A. Vasconcelos, G. Freddi and A. Cavaco-Paulo, *Biomacromolecules*, 2008, **9**, 1299-1305; (b) A. T. Quitain, H. Daimon, K. Fujie, S. Katoh and T. Moriyoshi, *Ind. Eng. Chem. Res.*, 2006, **45**, 4471-4474.
21 K. König, *J. Microsc.*, 2000, **200**, 83-104.
22 (a) K. Y. Pu, K. Li and B. Liu, *Adv. Mater.*, 2010, **22**, 643-646; (b) K. Y. Pu, K. Li, X. H. Zhang and B. Liu, *Adv. Mater.*, 2010, **22**, 4186-4189.
23 M. A. Albota, C. Xu and W. W. Webb, *Appl. Opt.*, 1998, **37**, 7352-7356.
24 S. Yao and K. D. Belfield, *J. Org. Chem.*, 2005, **70**, 5126-5132.
25 G. P. Bartholomew, M. Rumi, S. J. K. Pond, J. W. Perry, S. Tretiak and G. C. Bazan, *J. Am. Chem. Soc.*, 2004, **126**, 11529-11542.
26 Q. Q. Dang, S. D. Lu, S. Yu, P. C. Sun and Z. Yuan, *Biomacromolecules*, 2010, **11**, 1796-1801.
27 (a) Z. Z. Shao and F. Vollrath, *Nature*, 2002, **418**, 741-741; (b) J. H. Shi, S. X. Lua, N. Du, X. Y. Liu and J. X. Song, *Biomaterials*, 2008, **29**, 2820-2828.
28 (a) D. H. Kim, J. Viventi, J. J. Amsden, J. L. Xiao, L. Vigeland, Y. S. Kim, J. A. Blanco, B. Panilaitis, E. S. Frechette, D. Contreras, D. L. Kaplan, F. G. Omenetto, Y. G. Huang, K. C. Hwang, M. R. Zakin, B. Litt and J. A. Rogers, *Nat. Mater.*, 2010, **9**, 511-517; (b) F. V. David Porter, *Adv. Mater.*, 2009, **21**, 487-492; (c) N. Du, X. Y. Liu, J. Narayanan, L. A. Li, M. L. M. Lim and D. Q. Li, *Biophys. J.*, 2006, **91**, 4528-4535; (d) N. Du, Z. Yang, X. Y. Liu, Y. Li and H. Y. Xu, *Adv. Funct. Mater.*, 2011, **21**, 772-778.
29 (a) S. C. Yin, H. Y. Xu, W. F. Shi, Y. C. Gao, Y. L. Song and B. Z. Tang, *Dyes. Pigments*, 2006, **71**, 138-144; (b) L. C. Cesteros, J. R. Isasi and I. Katime, *Macromolecules*, 1993, **26**, 7256-7262.
30 G. S. He, Q. D. Zheng, K. T. Yong, F. Erogbogbo, M. T. Swihart and P. N. Prasad, *Nano Lett.*, 2008, **8**, 2688-2692.
31 X. H. Ouyang, H. P. Zeng and W. Ji, *J. Phys. Chem. B*, 2009, **113**, 14565-14573.